

Article

Simulation on the Effect of Porosity in the Elastic Modulus of SiC Particle Reinforced Al Matrix Composites

Jorge E. Rivera-Salinas ^{1,*}, Karla M. Gregorio-Jáuregui ², José A. Romero-Serrano ², Alejandro Cruz-Ramírez ² , Ernesto Hernández-Hernández ³, Argelia Miranda-Pérez ⁴  and Víctor H. Gutiérrez-Pérez ⁵

¹ Catedrático CONACyT—Department of Plastics Transformation Processing, Centro de Investigación en Química Aplicada—CIQA, 25294 Saltillo, Coahuila, Mexico

² Metallurgy and Materials Department, Instituto Politécnico Nacional, Escuela Superior de Ingeniería Química e Industrias Extractivas—ESIQIE, UPALM, 07738 México D.F., Mexico; kaarlaa@gmail.com (K.M.G.-J.); romeroipn@hotmail.com (J.A.R.-S.); alex73ipn@gmail.com (A.C.-R.)

³ Department of Advanced Materials. Centro de Investigación en Química Aplicada—CIQA, 25294 Saltillo, Coahuila, Mexico; ernesto.hernandez@ciqa.edu.mx

⁴ Corporación Mexicana de Investigación en Materiales S.A. de C.V., Ciencia y Tecnología—COMIMSA, 25290 Saltillo, Coahuila, Mexico; argelia.miranda@comimsa.com

⁵ Professional Specific Training Department. Instituto Politécnico Nacional—Unidad Profesional Interdisciplinaria de Ingeniería campus Zacatecas (UPIIZ), 98160 Zacatecas, Mexico; metalurgico2@hotmail.com

* Correspondence: enrique.rivera@ciqa.edu.mx; Tel.: +52-844-389-830

Received: 17 February 2020; Accepted: 14 March 2020; Published: 19 March 2020



Abstract: Although the porosity in Al-SiC metal matrix composites (MMC) can be diminished; its existence is unavoidable. The purpose of this work is to study the effect of porosity on Young's modulus of SiC reinforced aluminum matrix composites. Finite element analysis is performed based on the unit cell and the representative volume element approaches. The reliability of the models is validated by comparing the numerical predictions against several experimental data ranging in low- and high-volume fractions and good agreement is found. It is found that despite the stress transfer from the soft matrix to the reinforcement remains effective in the presence of pores, there is a drop in the stress gathering capability of the particles and thus, the resulting effective elastic modulus of composite decreases. The elastic property of the composite is more sensitive to pores away the reinforcement. It is confirmed, qualitatively, that the experimentally reported in the literature decrease in the elastic modulus is caused by the presence of pores.

Keywords: Al/SiC composite; porosity in composites; finite element analysis

1. Introduction

Particles embedded in a matrix are commonly encountered in metal matrixes since they arise during melt processing by non-controlled phase changes, mechanical interaction of the melt with its surroundings, or they are added intentionally as filler material. Stiff and soft particle inclusions in a matrix have effects that could be considered adverse or beneficial in the physical and mechanical properties of the bulk matrix. For example, hard particles in steel are considered harmful and they often originate the variability of steel properties [1]. On the other hand, the incorporation of ceramic stiffer particles—e.g., SiC, SiO₂, Al₂O₃, and WC—to matrixes such as aluminum alloys reinforce the bulk matrix and metal matrix composites (MMC) arise. Due to their high specific strength and

modulus, reinforced materials can be tailored, finding applications in multiple industries such as naval, aeronautics, automotive, and machining-tools. Moreover, MMC exhibit isotropic material properties [2].

The elastic properties of MMC depend principally on geometrical parameters: volume fraction, size distribution, shapes and stiffness of the particles, porosity, and bonding state at the interface. Studies have been conducted to elucidate the effects of particles embedded in metal matrixes [3,4], concluding that the shape of the particles influences the overall elastic response of the composite. While the particle size has no significant influence on the elastic modulus at low content of reinforcement [5,6].

For the microstructures having different phases like hard ceramic particles and pores, it is desirable to predict strength properties for the development of high-performance materials. Porosity in MMC can greatly influence the material properties and is mainly caused by manufacturing processes, thermal cycles, and both distribution and percentage particles [7–9]. For instance, enhancement of strength is affected in the interface causing crack initiation sites, which was evidenced in Hassani's study at varying milling times with different particle sizes and amounts. The visualization of porosity and voids employed specialized techniques such as nondestructive laser-ultrasonic spectroscopy where Podymova et al. [10] proposed a calibration curve for porosity evaluation as this defect compromise composite strength. Other techniques, such as neutron and synchrotron diffraction, where voids and pores are easily observed and micro stresses can be detected. Previous investigations conclude that thermal fatigue damage is produced by the porosity presence and can influence the coefficient of thermal expansion behavior in MMC, tensile and fatigue properties are also affected [8,11]. Consequently, porosity content decreases mechanical properties of MMC—such as tensile strength, Poisson ratio, and Young's modulus.

Modeling of inclusion-matrix interaction or pore-matrix interaction at the microscale is usefully in accurately predicting effective properties (e.g., Young's modulus). In the literature, several constitutive models (analytical, semi-empirical, differential, and variational methods) for the prediction of mechanical properties with specified volume fractions can be found elsewhere. Among these models, the ones proposed by Voigt and Reuss (V-R) [12,13] and by Hashin-Shtrikman (H-S) [14] have proven to be effective means to obtain upper and lower bounds for the elastic moduli of the MMC from the known properties of its constituents. The H-S model represents the tightest bounds. This model is based on variational principles of linear elasticity and assumes isotropic composite. None of the previous methods (V-R, H-S) consider microstructural information.

Micromechanical analytical models also have been established to predict the mechanical properties of porous solids. Ramakrishnan and Arunachalam (R-A) [15] derived a useful analytical model using the principles of statistical continuum mechanics, where the effective elastic moduli of bulk material are predicted as a function of the volume fraction of the pores, the variation of the effective Poisson's ratio, and the elastic modulus of the corresponding dense material. This model considers an assemblage of hollow spheres. Additional information about other theoretical models for porous solids and its validity can be found in [16]. It is difficult to derive analytical solutions for particle-pore interaction systems because the stress distribution around particles and pores start interfering with each other.

The finite element modeling of micromechanics is an alternative means to analytical models for the simulation of mechanical properties. Finite element analysis has become increasingly more popular and an accurate approach to study different phases and complex morphologies of reinforcement particles in the microstructures [1]. Approaches are the unit cell model (UC) and the representative volume element (REV). In the UC approach, one or two particles are embedded in the metal matrix to represent a periodical array since this approach assumes that the material microstructure is periodic. Because of the periodic assumption, the UC approach is computationally efficient. The REV approach assumes random microstructures. Studies on numerical modeling in MMC have simplified the morphology of the particle reinforcement to that of a circle, rectangle, or ellipse to study the elastic response of the composite [17,18]. Good correlation between the numerical predictions and the experimental data was obtained. Available theoretical studies have shown the effect of reinforcement volume fraction on the

stress distribution and modulus of MMC. However, such an understanding still lacks when particles interact with pores in MMC, where the presence of pore close to particle or even within the particle produces inhomogeneous stress distributions and the load-bearing capacity of MMC is affected.

On the other hand, in polymer matrix composites containing fibers, numerical studies have shown that the porosity has a much larger influence in transversal properties than the longitudinal ones and a critical volume fraction exists below when the strength is unaffected by pores [19]. For solders, the effects of the morphology of intermetallic and porosity volume fraction on the modulus of the solder were studied by Chawla et al. [20]. They used a 2D microstructure based finite element modeling to study the effect of the morphology of Ag_3Sn intermetallic and porosity on the Young's modulus of Sn–Ag solders. The Ag_3Sn morphology was controlled by cooling rate; spherical and needle-like particles were obtained. They conclude that the morphology of the particles should not have a significant influence on Young's modulus of the Ag-solder. Rather, the porosity is responsible for the variability of the elastic moduli. However, in this study the porosity effect was not included in the numerical model, instead, it analyzed with the (R–A) analytical model.

MMC porosity arises generally by causes of gas entrapment and the evolution of dissolved gases [21]. Although the porosity in MMC can be diminished, its existence is unavoidable [22]. As porosity causes structural weakness in particulate composites, this factor remains as one of the focuses to attract researchers' attention in the development of high-performance materials. Ray [23] classified porosity of composites in two types: (a) at the boundary of the matrix phase and the reinforcement, and (b) away from the filler particles in the matrix alloy. In the works of Sun et al. [24] and Podymova et al. [10], it was found that pores coexist with the clustered and large-sized particles, and they significantly decrease the mechanical properties of the composites. The porosity in MMC arises from different origins, therefore it is of great interest to screening the inhomogeneous stress field around pores interacting with hard particles, and how the discontinuity produced by the pores has a damaging effect on the load-bearing capacity of the MMC. Finite element analysis is a means of properly interpreting the effect of porosity on the elastic properties of porous materials [16,19]. This paper aims to investigate the effect of porosity on the elastic modulus of SiC particle reinforced Al matrix composites. Finite element models based on the UC and REV approaches were developed. Porosity is considered within the Al matrix and within SiC particle to determine how the load-bearing capacity of the composite is affected by the different regions of stress concentration origins. The shapes of the reinforcement particle are angular and circular in the UC approach. Whereas, in the REV approach, the microstructures were developed to incorporate the mechanical interaction between the reinforcing particles. Firstly, the numerical methodology is validated against experimental data available in the literature ranging in a low and high-volume fraction of reinforcement. Also, the constitutive models of H–S, V–R, and R–A are used for reference.

2. Numerical Modeling

Square and circular morphologies of the particle reinforcement were selected to elucidate the effect of the inclusion shape in the elastic moduli. Two validation studies are conducted first by comparing the FEA results within experimental data reported for the system Co–WC [25] and experimental results for porous refractory spinel [16]. In the case of matrix strengthening, the composite matrix is made of cobalt (Co), whose elastic modulus $E_2 = 207$ [GPa], Poisson's ratio $\eta_2 = 0.31$ and shear modulus $G_2 = 79$ [GPa]. The inclusion is tungsten carbide (WC) whose elastic modulus $E_1 = 700$ [GPa], Poisson's ratio $\eta_1 = 0.23$, and shear modulus $G_1 = 278$ [GPa]. For the Co–WC composite, experimental data of the elastic moduli as a function of the volume fraction of reinforcement ranging at high concentrations of filler are available in the literature [25]. Therefore, this data allows examining the reliability of the numerical model when high volume fractions are considered. As the volume fraction of the reinforcement increases, advanced micromechanical models are needed [26].

In the case of the porous material, the elastic modulus and Poisson's ratio of MgAl_2O_4 are $E_{\text{spinel}} = 268.2$ [GPa] and $\nu_0 = 0.262$, respectively. For modeling the pore, zero-moduli and zero-Poisson's ratio

are assigned appropriately to avoid singularities in the numerical model. For computing the effective elastic moduli of the materials, two-dimensional (2D) UCs models of 8×8 mm with a different volume fraction of the reinforcement and porosity were created. Plane strain behavior is assumed. In the case of the UCs models the center of mass of the reinforcement particles coincides with that of the square representing the matrix. Pores are introduced explicitly in the metal matrix and within the particle reinforcement. Since the model is 2D, the volume fraction is equal to that of area fraction. The sizes of the particles are varied to obtain different volume fractions. For the REV models, the volume fraction and particle sizes are fixed. The unit cell is under tensile loading.

2.1. Linear Elasticity Equations

The governing equations for the static mechanic's problem are given by the equilibrium equation

$$\nabla \cdot \boldsymbol{\sigma} + \mathbf{f} = 0 \quad (1)$$

where, $\boldsymbol{\sigma}$ and \mathbf{f} are the stress tensor and body force, respectively. For the stress-strain relation, it is assumed a plane strain model. Therefore, strain normal to the plane is zero, and shear strains that involve angles normal to the plane are assumed to vanish. Constituent materials are isotropic, so the constitutive equation ($\boldsymbol{\sigma} = \mathbf{D}\boldsymbol{\varepsilon}$) is given by [27]

$$\mathbf{D} = \frac{E}{(1+\nu)(1+2\nu)} \begin{bmatrix} 1-\nu & \nu & 0 \\ \nu & 1-\nu & 0 \\ 0 & 0 & (1-2\nu)/2 \end{bmatrix} \quad (2)$$

where E is the Young's modulus and ν the Poisson's ratio. Macroscopically, the heterogeneous material can be assumed as a homogenous medium. The average strains, stress and strain in the composite are related to the boundary displacements of the UC and the REV by Gauss theorem. Therefore, using appropriate boundary conditions to produce uniform stress and strain in the homogeneous medium, the relation between the actual heterogeneous composite and the homogeneous medium is given by averaging the stress and strain tensors over the area of the unit cell [28].

$$\bar{\sigma}_{ij} = \frac{1}{A} \int_A \sigma_{ij}(x, y) dA = \frac{1}{A} \int_{\Gamma} (Eu_i n_j + Eu_j n_i) d\Gamma \quad (3)$$

$$\bar{\varepsilon}_{ij} = \frac{1}{A} \int_A \varepsilon_{ij}(x, y) dA = \frac{1}{A} \int_{\Gamma} (u_i n_j + u_j n_i) d\Gamma \quad (4)$$

The effective elastic moduli of the metal matrix composite (E_c), is given by substitution of the two previous equations into the Hook's law $\bar{\sigma}_{ij} = E_c \bar{\varepsilon}_{ij}$.

2.2. Finite Element Implementation

The 2D numerical models are developed using the mechanic's module in the software COMSOL Multiphysics. Boundary conditions assume plane strain-tension to evaluate the elastic modulus of the composites. Figure 1 shows the boundary conditions and the periodic microstructures that are considered for the UCs models. The mesh refinement is applied to ensure mesh independent solutions for each microstructure. The inclusion volume fraction is varied by changing the inclusion size in a parametric study, where the circular reinforcement is only able of producing volume fraction up to 0.71% while the square reinforcement a maximum volume fraction of 0.91%. The external load \mathbf{F} is set to 0.1 Pa. The microstructures used in the REV approach are shown in Section 3.2.5. This latter study was performed to compare the mechanical behavior predicted by the UCs models, with that predicted by the structure of real composite material. The boundary conditions are the same as those used in the UCs models.

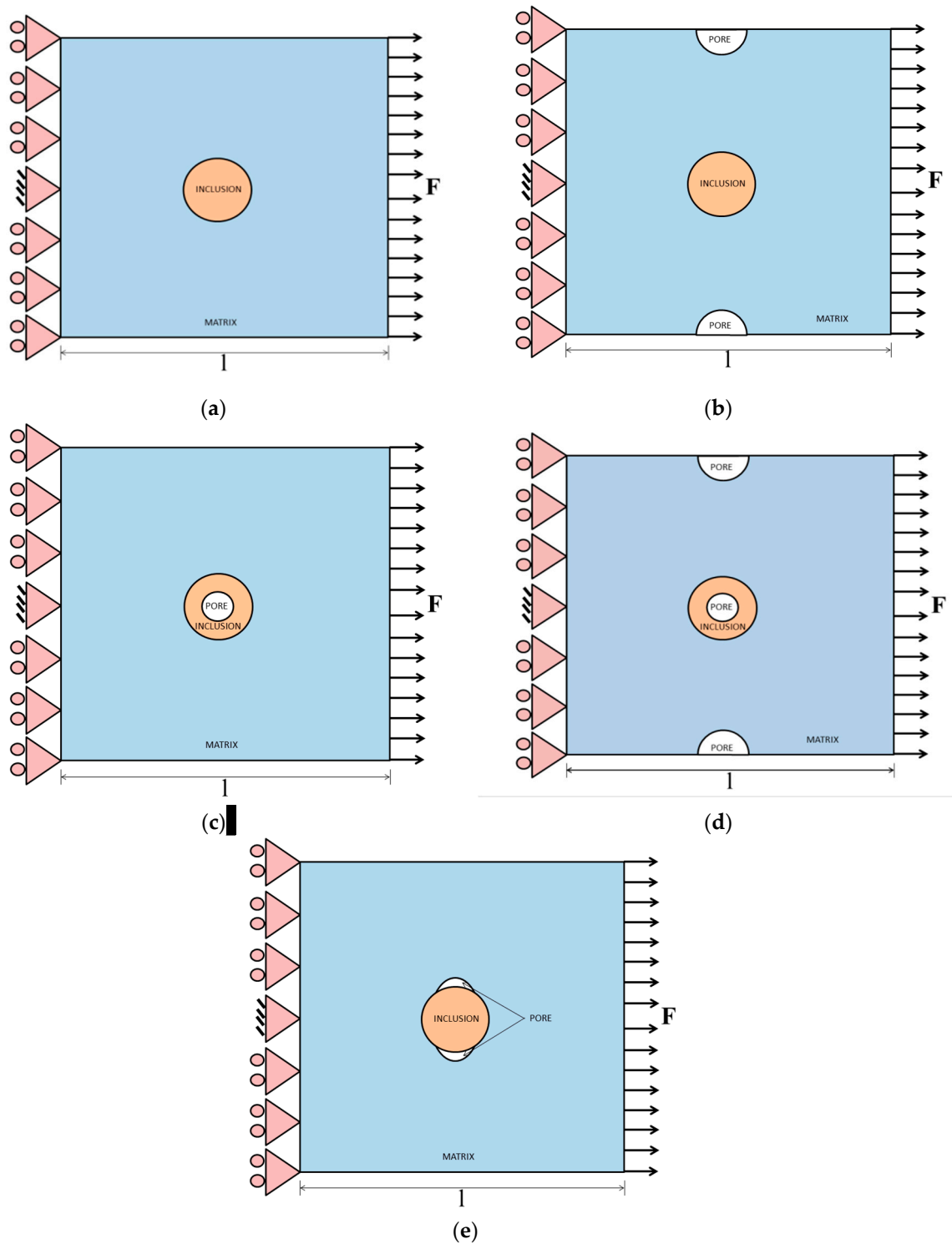


Figure 1. Schematic representation of the unit cell model and its boundary conditions. Particle reinforcements are considered square and circular. (a) Pore free matrix and pore-free particle. (b) Porous matrix and pore-free particle. (c) Pore free matrix and porous particle and (d) porous matrix and porous particle. (e) Porosity at particle–matrix interface. The triangles on the left side represent constraints displacement in the node.

3. Results and Discussions

3.1. Comparison of FEA Predictions with Experimental Data

The numerical methodology was validated by comparing the numerical effective elastic modulus of the composites against experimental data published for the cemented carbides, which consist of WC particles distributed in cobalt [25]. This study considers small and large granules, with reinforcement volume fraction ranging from 50–90% and the elastic modulus were determined by resonant ultrasound spectroscopy (RUS) and impulse excitation. The elastic modulus predicted from the bounds of Hashin–Shtrikman (H–S) and Voigt–Reuss (V–R) is also used as a reference. The H–S micromechanical model is perhaps the most widely used because of its accuracy. Bounds are the tightest possible ones from a range of composite moduli; the two-phase material moduli can be obtained as

$$E^{\pm} = E_2 + \frac{\phi_1}{1/(E_1 - E_2) + (3\phi_2/(3E_2 + 4G_2))} \quad (5)$$

For the computation of the upper bound $E_2 > E_1$, meanwhile, the lower bound is computed by interchanging the subscripts (1,2) in the previous equation. Here, E is the Young's modulus, G is the shear moduli, and ϕ is the volume fraction.

Figure 2 shows the comparison between H–S bounds on the Young's modulus for the Co/WC system, experimental results [25] and numerical data obtained by simplifying the actual particle morphology to a square and a circle. V–R bounds are also plotted for reference. It is seen that the numerical predictions fall within the H–S bounds and that the square capture the angular nature of the WC particles since these data are closer to the experimental values (WC particles are angular). However, at the volume fraction of filler of 91%, the numerical prediction lies above the H–S upper bound. The numerical error was evaluated as $\left| \frac{(E_{HS}^+ - E_{numerical})}{E_{HS}^+} \right|$, which is lower than 3% at the volume fraction of 91% with $E_{numerical} = 655$ [GPa] and $E_{HS}^+ = 638$ [GPa]. Whenever the numerical predictions do not overtake the (V–R) bounds, the predictions are considered valid [29]. The upper bound of the V–R bounds is just 655 [GPa] at the volume fraction of 91%, so the numerical prediction lies at the upper bound of the V–R model and does not overtake this bound. This confirms that the predictions for the elastic moduli from the UC models developed are reliable. Results also show that the square particle has a little greater stiffening effect than the circular particles. Since the square particle values are close to the experimental ones, no additional effort was undertaken to consider a polygonal shape of the inclusion.

The information plotted in Figure 2 shows that the numerical model correctly predicts the stiffening effect. The validity of the developed numerical methodology was evaluated for the prediction of the effective Young's moduli when one phase of the composite has a zero-moduli and zero-Poisson's ratio. The analytical model for micromechanics of porous mediums proposed by Ramakrishnan and Arunachalam (R–A) was used as a reference. Experimental data reported in [16] was used to determine the accuracy of the numerical methodology in capturing the presence of pores in the composite. The R–A model was established considering that the dispersed phase of the composite has zero moduli, which means that in the porous area, the stress is zero but not the strain, the equations that describe this behavior are the following

$$E^* = E(1 - \theta)^2 / (1 + b_{\theta}\theta) \quad (6)$$

$$b_{\theta} = 2 - 3\nu_0 \quad (7)$$

where E is the Young's modulus of the fully dense material, θ the porosity, and b_{θ} is a constant that depends on the Poisson's ratio ν_0 of fully dense material.

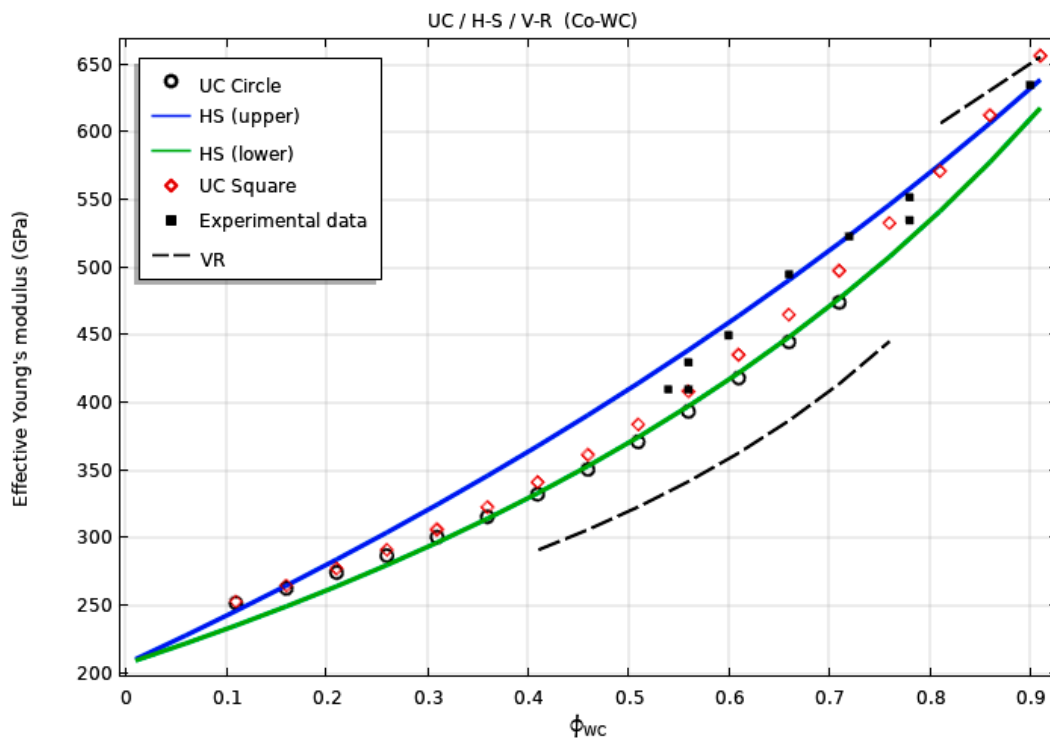


Figure 2. H–S bounds (—), experimental data (■) [25], numerical data (square ◊, circle ○) and V–R bounds (---) for the Young’s modulus for Co–WC system.

Numerical results were compared to the experimental data for the porous refractory spinel, where the effective elastic modulus was determined in [16] as a function of the porosity ranging from a fully dense material up to 40% porosity. Figure 3 shows this comparison when the pore shapes are circular and square to reflect the effect of pore shape on the Young’s moduli. The circular porous geometry fit the experimental data better than that of the square one. Since the simulation results with a circular pore show a close match to experimental data, the pore geometry considered in the UC models is only circular. The comparison between numerical results and experimental data shows that the present numerical models developed are also reliable when zero moduli and zero-Poisson’s ratio are assigned for one phase in the heterogeneous material. The computed results show that the UC model calculations are in good agreement with experimental data available in the literature [16,25] which proves the validity of the presented approach for microstructures of two phases. However, it is necessary to be careful when considering a three-phase material since it is necessary to place an inclusion (particle or pore) out from the center of mass of the UC model. In this work, pores are placed in the boundary, at the center of the UC and both the boundary and the center of the UC. In order to take into care that the composite behavior is not dominated by the boundary conditions (Saint-Venant’s principle), the influence of pore location on the computed elastic modulus was first established. As mentioned above, when the pore is in the center of mass of the UC, the numerical results are close to the experimental data in a wide range of values of pore content (Figure 3). On the other hand, when the pores are placed on the boundaries of the unit cell, the model predictions are reliable only when the pore content is ranging in low volume fraction as shown in Figure 4. Besides, it is observed that the model predictions are reliable when considering porosity up to 14% with a maximal deviation $((E_{exp} - E_{FEM})/E_{exp})$ of 6.6%. Thus, to interpret the numerical results properly when the pore is out from the center of mass of the UC, pore content should be lower than 14%. It is assumed that similar accuracy pertains when the numerical methodology is used to find the local stress and strain for the porous (Al/SiC) composites.

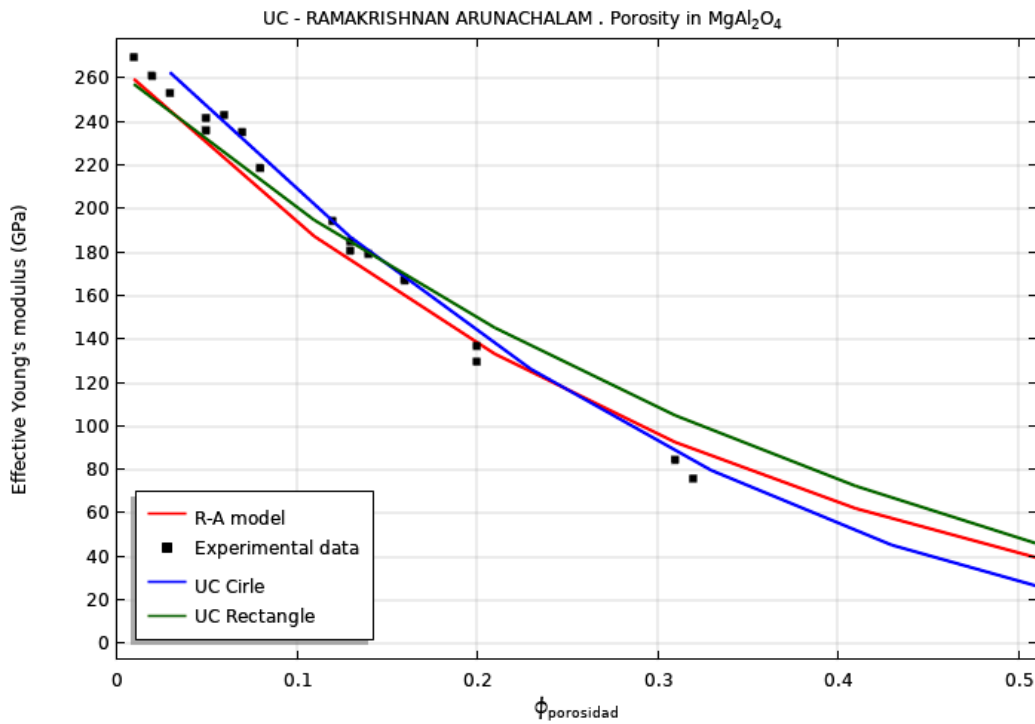


Figure 3. Variation of the effective elastic moduli for porous spinel. R–A model (—), experimental data (■) [16] and numerical data (square —, circle —).

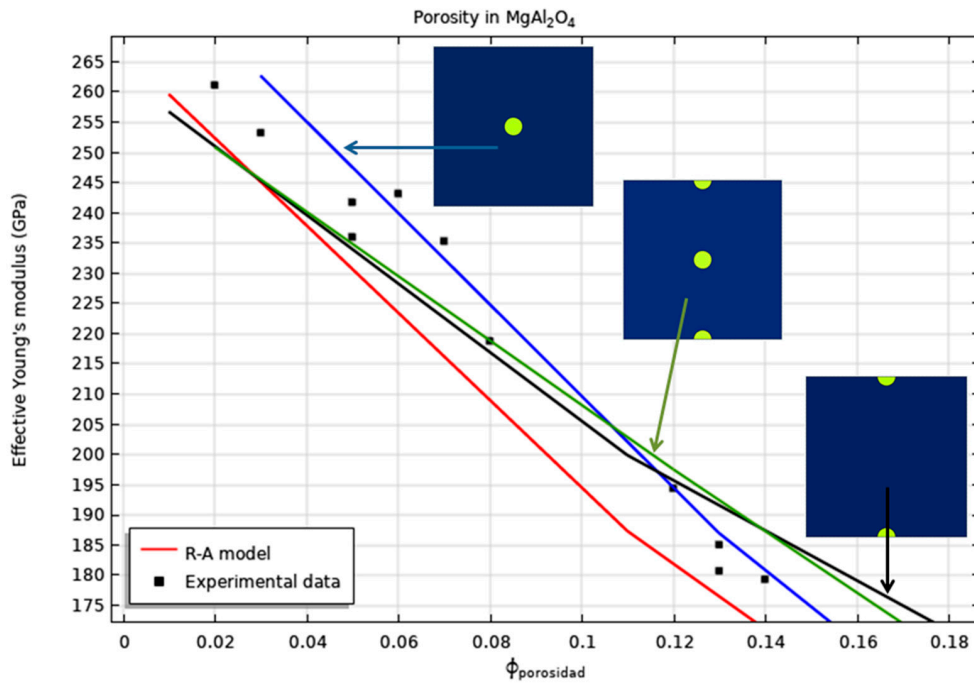


Figure 4. Influence of pore location on the numerical predictions of the elastic modulus. When the pore is placed at the center of mass, the model is reliable for a wide range of porous volume fraction. On the other hand, when the pores are placed in the boundaries of the UC, the model is reliable for porosity content ranging from 0% to 14% with an error lower to 7%.

3.2. SiC Particle Reinforced Aluminum Composites

Aluminum matrix composites possess both structural and functional applications, as a result, they are being increasingly used in several industries such as automotive; however, with the current

manufacturing process, it is difficult to avoid the porosity in MMC. Moreover, the porosity arises from different origins [10,23,24]. Therefore, the porosity has different destructive effects on the strength of the MMC. This factor has attracted the interest of the current research to investigate the effect of the porosity using finite element analysis on the load-bearing capacity of Al/SiC composites. The numerical models based on the microstructures shown in Figure 1 were constructed. The shape of the SiC particle is considered square and circular to determine the strengthening effect due to the particle's shape. The mechanical properties of the particle and matrix are shown in Table 1 [30]. The results are shown in the next section.

Table 1. Material properties of the SiC particle and Al matrix [30].

Material	Young's Modulus (GPa)	Poisson's Ratio
Al	74	0.33
SiC	410	0.19

3.2.1. Pore-Free Al-Matrix and Pore-Free SiC-Particle

Figure 5 illustrates the surface plots of von Mises stress in the microstructure when the particle and matrix are fully dense. Both unit cells (square and circular SiC-particle) are under the same external load and the volume fraction of reinforcement is 0.26%. For the SiC square particle (Figure 5a) the maximum stress value in the particle is 0.4 Pa, this stress is mainly concentrated at the corners of the particle. In the case of the circular SiC particle (Figure 5b), its maximum stress value is 0.11 Pa, which is concentrated at the contour of the particle. A comparison of both the square and circle particles shows that the stress gradient at the interface of the particle-matrix is larger when the reinforcement shape is angular (Figure 5a) than when is circular (Figure 5b). In both cases, the stress in the particle is larger than the stress in the matrix. Regarding the deformation in the composite, the strain in the matrix is larger than that of the particle because the particles are stiffer than the matrix. Based in the fact that the external load must equal the sum of the volume-averaged loads borne by the constituents (matrix and reinforcement). Then, if the reinforcement carries a relatively high proportion of the externally applied load, it is regarded as acting efficiently ($\sigma_c = \sigma_m(1 - \phi) + \sigma_p\phi$) [31]. Then, the load is better transferred from the soft Al-matrix to the hard SiC particles when angular particles are used as reinforcement. These results agree with that reported in [17], where the load transfer by a shear-lag type of mechanism is more effective across planar interfaces than a spherical interface.

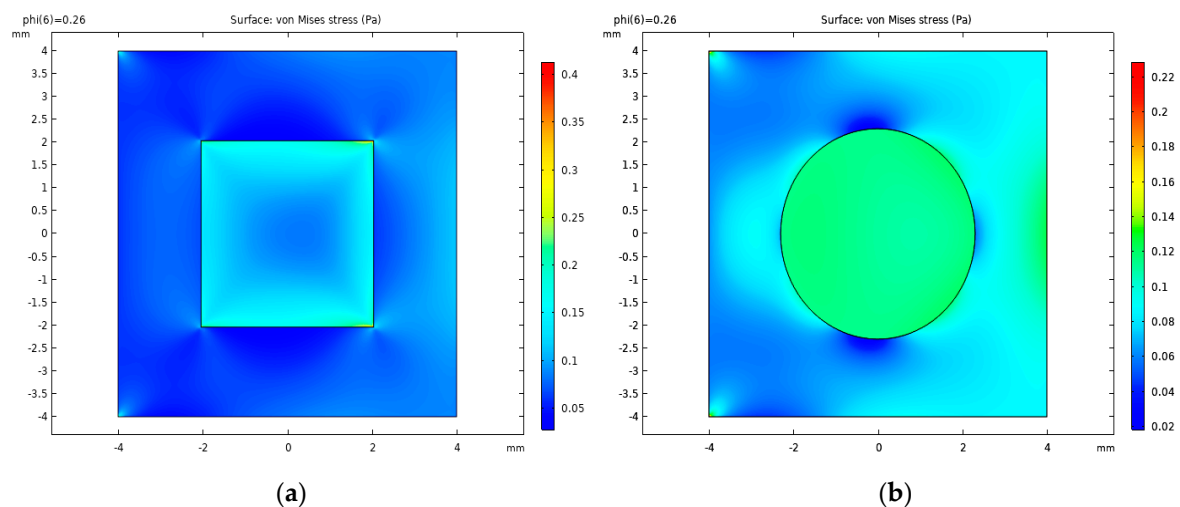


Figure 5. Surface plots of von Mises stress for the composite reinforced by SiC particles of (a) square shape and (b) circular shape. The volume fraction of reinforcement is 0.26%.

Figure 6 shows that, at low volume fractions of particle reinforcement, the effective elastic modulus of the circular particles composite is like that obtained with angular particles (red and black dashed lines). Then, the amount of transfer external-load from the matrix to the particle reinforcement at low volume fractions of SiC particles is similar for angular than circular particles. Therefore, at low volume reinforcement content, the particle shape has little effect on the elastic modulus of the composite. Figure 6 also shows the comparison between H–S bounds on Young’s modulus for the Al/SiC system with data from various Al/SiC MMCs experimental results [32–37] and the numerical data obtained in this study. In the plot, the gathered experimental data—as well as the numerical predictions on the Young’s modulus of the composite—lies near the lower bound of the H–S model. Therefore, the prediction on the strength of the Al-SiC composites can be done with a high level of confidence using the lower bound of the H–S micromechanical model. Numerical predictions of the elastic modulus based on the square and circular SiC particles are very close to the reported measured data for the Al alloy-SiC systems. As the volume fraction of SiC increases, angular particles strengthen the composite better than the circular ones do. According to the H–S lower bound, the circular shape in the numerical model underpredicts the elastic modulus of the Al-SiC composite. Though these predictions (with circular particles) fall off from the H–S lower bound, the data reported by Qu et al. [34] demonstrates that the numerical predictions are reliable and the condition proposed in [29], is confirmed; while the V–R bounds are not overtaken, the numerical model is reliable. However, the accuracy of the numerical results must be checked by comparing the results to experimental data.

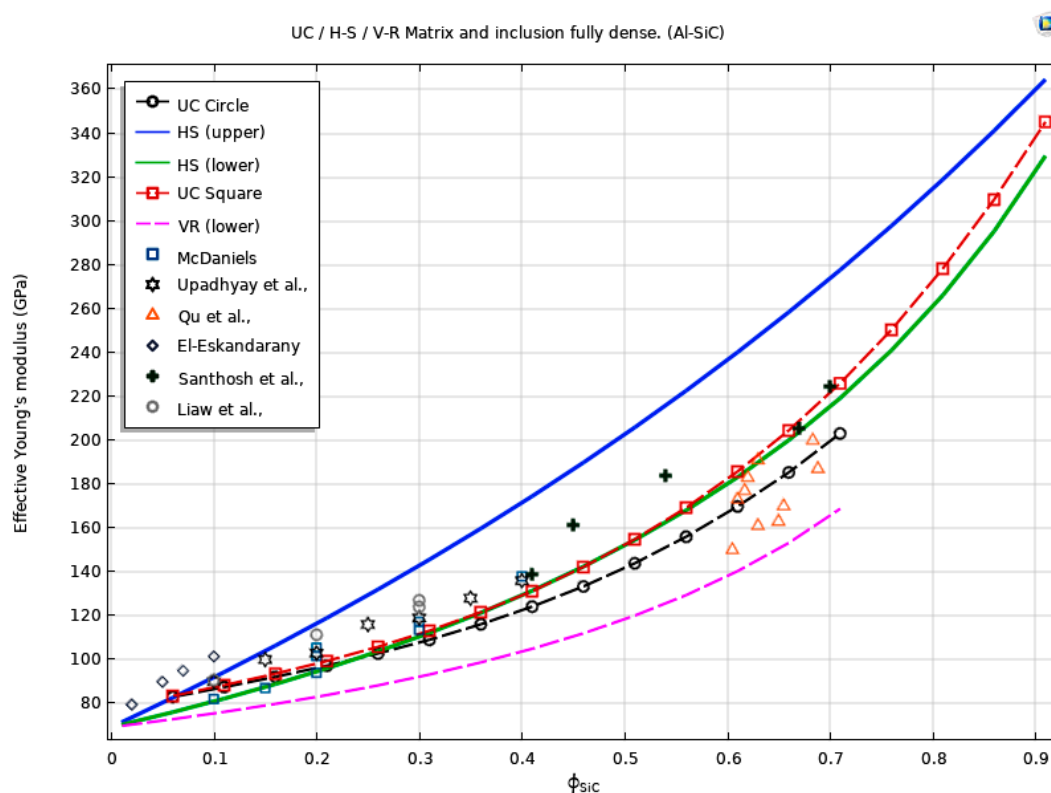


Figure 6. Effect of reinforcement content on the elastic modulus of Al-SiC composite. H–S bounds (—), experimental data [32–37], numerical data (square ■, circle ●) and V–R bounds (---).

The SiC square or angular particle reinforced Al matrix composites endure more load than reinforced with SiC round particles as shown in Figure 7. This plot shows the stress ratio (stress in the particle and the stress in the matrix, σ_p/σ_m) as a function of the reinforcement volume fraction. It is considered that the composite remains elastic independently of the applied load [31]. It is found that the square and circular particles endure the same load to the volume fraction up to 11%. However,

above this reinforcement content, the angular particle endures more load. Then, the effective elastic modulus of the MMC is independent of the particle morphology when the reinforcement content is lower than 11%.

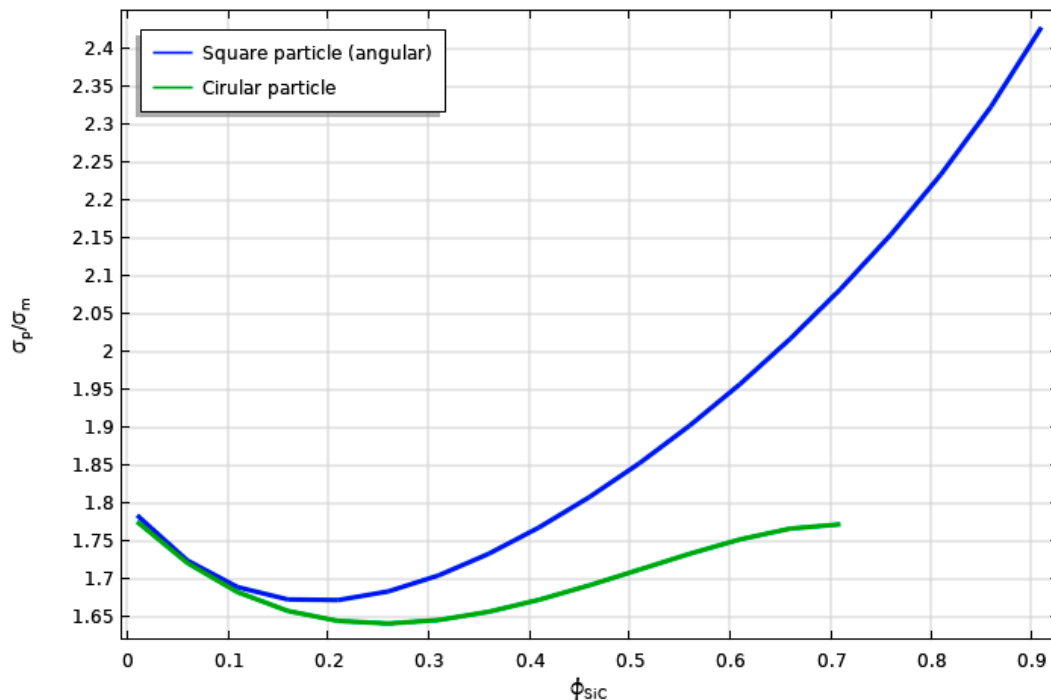


Figure 7. The portion of the external load borne by each of the constituents of the composite. Square particle (blue) and circular particle (green).

3.2.2. Porous Al-Matrix and Pore-Free SiC Particle

The porosity significantly affects the mechanical performance of the composites. The porosity increases as the weighting percentage of particles increases. In [21] it was found that the porosity content of the Al composites varied from 1.01% to 2.69% with the increased SiC wt % from 0% to 25%. A parametric study was performed, where a similar increase-relationship between the amount of porosity and the content of SiC particles is maintained; where the porosity increases as the volume fraction of reinforcement do. Porosity content (volume fraction) varies from 0% to 3.1% with SiC particle added from 1% to 31%. Figure 8 shows the surface plots of von Mises stress in the microstructure when the Al-matrix is porous, and the SiC-particle is fully dense. These results are based on the microstructure shown in Figure 1b. The maximum stress obtained in the square particle is about 0.5 MPa (Figure 8a). Whereas, for the circular particle, the maximum stress in the particle is 0.14 MPa (Figure 8b). In both Al-matrixes (square and circular particle) high-stress concentration around the pore is observed, with a value of about 0.2 MPa, however, the stress in the matrix is bigger than the stress in the particle in the case of the circular reinforcement. As the stress in the SiC square particle is higher than that of the Al-matrix, the load transfer remains effective despite the presence of pores in the Al-matrix. In Figure 8b it is shown that the stress gradient at the interface of the SiC circular particle and Al-matrix is low; namely at some points of the interface, the matrix and the reinforcement endure the same load.

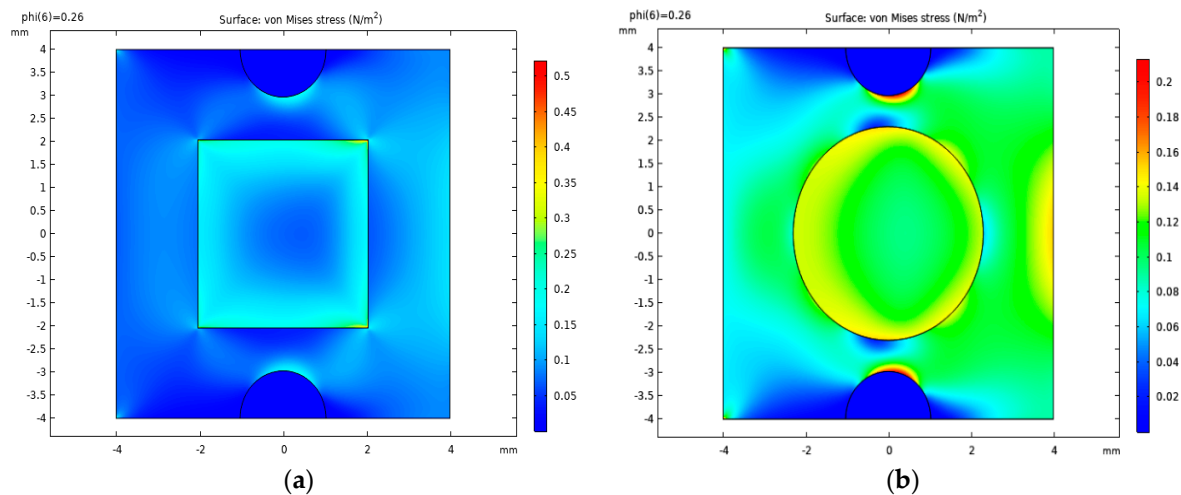


Figure 8. Von-Mises stress distribution of 26% SiC particulate filled porous-aluminum matrix under tensile loading. (a) Square shape and (b) circular shape.

3.2.3. Pore Free Al-matrix and Porous SiC Particle

Figure 9 shows the surface plots von Mises stress in the microstructure when the Al-matrix is fully dense, and the SiC-particle is porous. These results are based on the microstructure shown in Figure 1c. For the square porous particle (Figure 9a), the stress in the particle (maximum stress 0.44 Pa) is greater than the stress in the matrix, which shows that strengthening of the composite is by transfer load from the soft Al-matrix to the SiC hard particle. The stress concentration around the pore within the particle is 0.35 Pa, while the stress located in the angles of the particle is 0.44 Pa. In the case of the SiC circular particle (Figure 9b), the maximum stress in the particle is around the pore with a value of 0.42 Pa, while in the Al-matrix the stress is lower, so transfer load is also effective in this case. Stress concentration around the pore is higher for the circular particles than square particles, which means that circular porous particles are more prone to fracture than angular porous particles when pores coexist inside the particles.

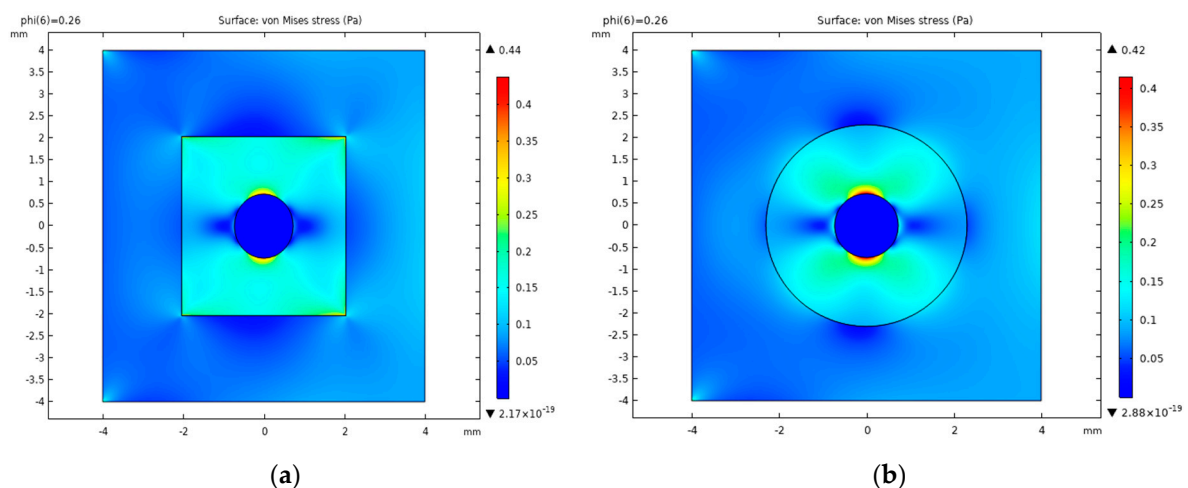


Figure 9. Von Mises stress distribution of SiC porous-particulate filled aluminum matrix under tensile loading. (a) Square shape and (b) circular shape. The volume fraction of SiC particles and pore content is 26% and 2.6%, respectively.

3.2.4. Porous Al-Matrix and Porous SiC Particle

Figure 10 shows the surface plots of von Mises stress in the microstructure when the Al-matrix and the SiC-particle are both porous. These results are based on the microstructure shown in Figure 1d. In this case, the total porosity is divided into an equal content in the matrix and the particle; so, the pore content in the matrix is 1.3%, while the pore content in the particle is 1.3%. The total pore content in the composite is 2.6%. Figure 10a,b show that the stress concentration around the pore in the Al-matrix is about 0.2 Pa in both cases (the square particle and circular one). However, the stress around the pore in the SiC particle reinforcement is bigger for the circular particle (0.39 Pa) than the stress in the pore located in the square particle (0.31 Pa). Therefore, when the matrix is porous, the stress gathering around the pore within the particles is lower than when the matrix is fully dense. That means that the pore in the matrix reduces the transfer load mechanism and more load is endured by the matrix lowering the strengthening of the composite. For the square SiC particle, the maximum stress (in the corners) is 0.5 Pa, while the stress in the Al-matrix is 0.2 Pa, this shows that the transfer load mechanism from the matrix to the reinforcement remains despite the pore presence at the matrix and particle.

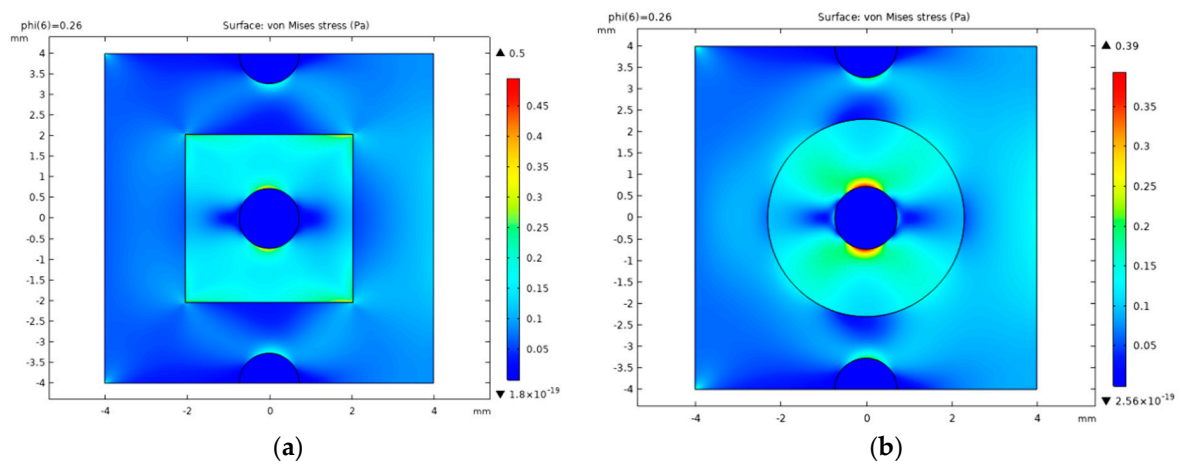


Figure 10. Von Mises stress distribution of SiC porous-particulate filled porous aluminum matrix under tensile loading. (a) Square shape and (b) circular shape. The volume fraction of SiC particles and pore content is 26% and 2.6%, respectively.

3.2.5. Porosity at Matrix–Particle Interface

Figure 11 shows the surface plots of von Mises stress in the microstructure when the pore is located at the particle–matrix interface. For the square particle (Figure 11a), the stress in the particle (0.3 Pa) is greater than the stress in the matrix (0.09 Pa), which shows that strengthening of the composite is by transfer load from the soft Al-matrix to the SiC hard particle. The stress is concentrated at the particle corners, but the highest stress concentration (0.5 Pa) is located at some contact points between the particle, matrix, and pore. In the case of the SiC circular particle (Figure 11b), the stress concentration is at all the contact points among the particle, matrix, and pore, and when compared to the square particle, the stress intensity is two-fold. Moreover, the stress level in the particle (0.13 Pa) is a little bit greater than that in the matrix (0.11 Pa). Therefore, in the case of the circular particles, the pores located at the particle–matrix interface significantly affect the transfer load mechanism, whereas in the case of the angular particles, the transfer load remains effective still because a relatively high proportion of the externally applied load is endured by the particle. As mentioned in Ray [23] this type of porosity aid the debonding of particles from the matrix under low stress, because the interface damage starts to develop since the contact points among the particle matrix and the pores act as a stress concentrator, as shown here.

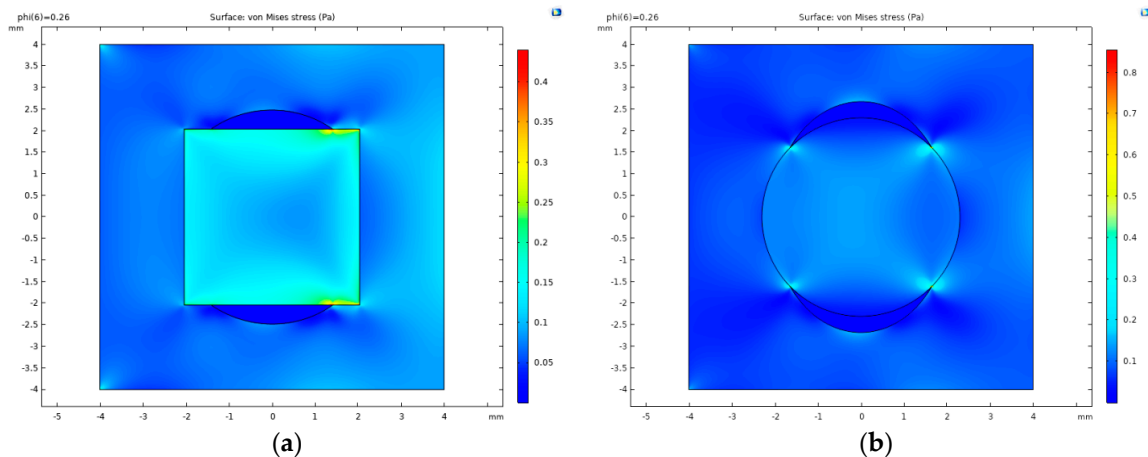


Figure 11. Surface plots of the von Mises stress for the composite reinforced by SiC particles of (a) square shape and (b) circular shape. The volume fraction of SiC particles and pore content is 26% and 2.6%, respectively. Porosity at particle–matrix interface.

It is found that square particles carry much higher stress than matrix in the case of porous matrix and fully dense particle (Figure 8a). Whereas, in the case of the circular particle, it carries much higher stress than matrix when the particle is porous, and the matrix is fully dense (Figure 9b). From the previous results, it can be seen that despite the presence of pore in the composite, stress transfer from the soft matrix to the hard particle is effective in all cases, except in the case of fully dense circular particle and porous matrix (Figure 8b), where the matrix endures more load than the particle. Then, the transfer load is lowered, and this is reflected as a reduction in the elastic modulus of the composite (Figure 12, black line with circular markers). Figure 12 shows the results gathered from the parametric study to demonstrate the effect of the porosity in the elastic modulus of the SiC particle reinforced Al matrix. In this parametric study, porosity content varies from 0% to 3.1% with SiC particle added from 1% to 31%. For the studied cases that consider coexistence of pores inside the particle and the matrix, the greater impairing on the Young's modulus of the composite was found to be in the case of the fully dense particle and porous matrix. The lower impairing on the elastic modulus of the composite is for the porous particle and fully dense matrix. Intermediate values on the impairing of the Young's modulus of the composite are for the case of porous particle and porous matrix, as well as the pore located at particle–matrix interface when the particle is circular. For the square or angular particles, the pore within the particle affects the load transfer mechanism in a similar manner to the pore located at the particle matrix interface. These results mean that the elastic property of the composite is more sensitive to the porosity in the matrix because the particles are stiffer than the matrix. The declining trend for the elastic moduli is consistent in both the angular and circular particle shapes. In all cases, the square or angular particles strengthen the composite when compared to the circular particles. From the results, it is concluded that the disrupting of continuity in the composite by the presence of pores causes elastic relaxation of the matrix, which leads to the reinforcement particles (angular or circular) undergoing increased loads. Consequently, this leads to a relaxation in the particle, and there is a drop in its stress gathering capability, and thus the resulting effective elastic modulus of the Al/SiC composite decreases. Therefore, the data indicate that the porosity in the composite matrix is the main cause in the impairing of the elastic modulus in MMC. In practice, the scatter of experimental data on the elastic modulus is caused mainly by the porosity in the composite because the difficult of experimentally reproducing the same porosity in the composite every test. Table 2 shows how the % increment in porosity in the matrix reduces the elastic modulus of the composite. Moreover, despite the volume fraction of the reinforcement is increased, if the porosity increase, the impairing on the Young's modulus is increased also. Therefore, the porosity plays a significant role in the strength of the

composites, and for a given porosity in the matrix, it impairs the Young’s modulus in the same way independently of the shape of the SiC-reinforcement.

Table 2. Porosity increase in the Al-matrix and its effect on the Young’s modulus of the composite.

SiC Volume Fraction	10%	-	20%	-	30%	-
Shape of the Particle	1% in porosity	% reduction	2% in porosity	% reduction	3% in porosity	% reduction
Square	88.2 GPa * 80.8 GPa †	8.3	99.3 GPa * 85.1 GPa †	14.3	113.15 GPa * 94.7 GPa †	16.3
Circular	87.3 GPa * 80.0 GPa †	8.3	97.1 GPa * 82.9 GPa †	14.6	109.0 GPa * 90.2 GPa †	17.2

* Pore-free matrix † Porous matrix.

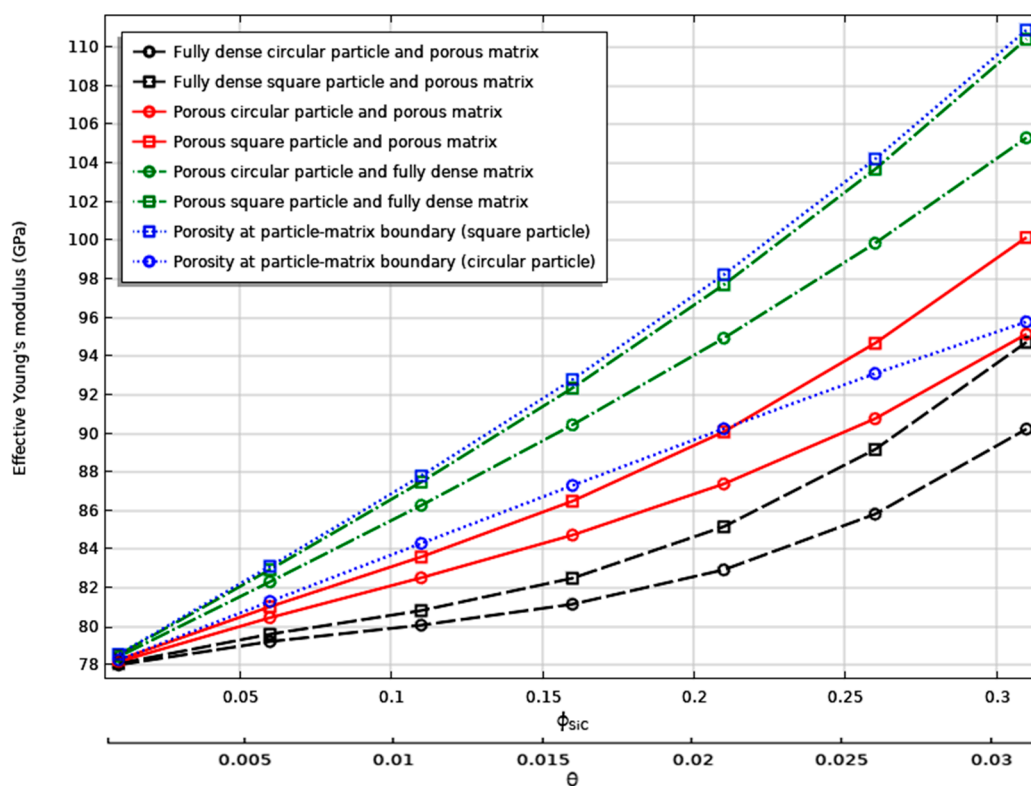


Figure 12. Effect of porosity in the elastic modulus of the Al-SiC composite. ϕ_{SiC} is the reinforcing content and θ is the porosity content in the composite. Square markers are for the square particle while circular markers are for the circular particle.

3.2.6. REV Models with SiC Particles Representing 2D Real Microstructures

The effective material properties are linked to the microstructure of composite. Therefore, the global behavior of the material depends on the microstructure, and modeling of the microstructure is as important as the prediction of global behavior. To visualize the difference between the material properties predictions conducted by assuming a single SiC particle of simple geometry in a unit cell, and those predictions of a cell model with several SiC particles exhibiting statistical homogeneity and isotropy as the real microstructures. Thus, two cell models (REV approach) that display distribution and orientation of particles of different sizes and shapes are established. The interactions between the particles produce a complicated local stress field with high stress concentrations which depends on the particle morphology. Figure 13 shows the developed microstructures. By comparing these

microstructures with the experimentally obtained microstructures for SiC reinforced Al matrix composites reported elsewhere, they are quite similar in the context that the position of the polygonal particles are randomly defined, the particles present different sizes, shapes, and orientation. Hence, these microstructures capture the same complicated mechanical interactions as the experimental ones will do. The volume fraction of reinforcement is 12% (Figure 13a) whereas the pore content is 1.2% in volume fraction (Figure 13b). The finite element implementation of these unit cell models is the same followed in Section 2.2, with the main difference that in this section, a parametric study is not needed, due to the volume fraction of the constituents is fixed. It is important to note that despite the shape of some pores look like a circle, they are not perfectly circular.

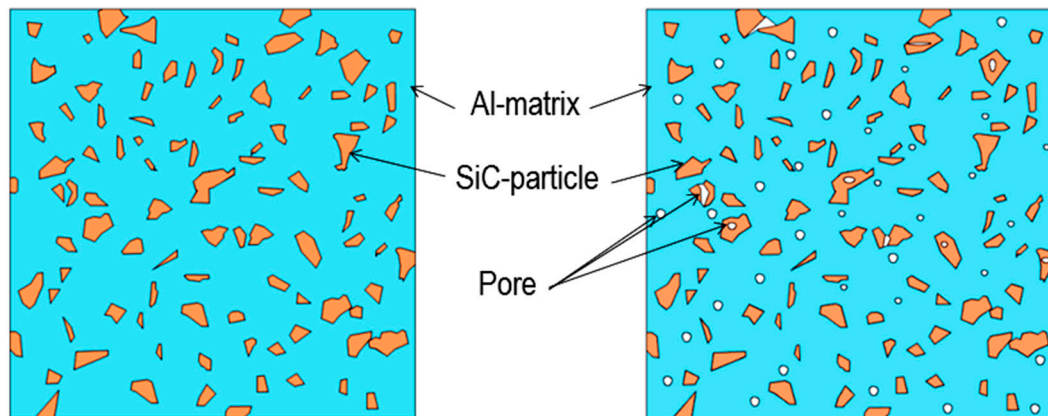


Figure 13. Developed microstructures for Al-SiC composite. (a) Fully dense materials and (b) porous materials.

Figure 14a,b show the surface plots of von Mises stress in the Al-matrix and the SiC particles, respectively. The stress in the particles is larger than in the matrix, and the stress in the particles is mainly concentrated in the sharp angular corners. These results are in agreement with the stress fields shown previously in Sections 3.2.1–3.2.5. Moreover, the stress field magnitudes are similar for the matrix as well as for the particles. The Young's modulus of the composite using this microstructure is 91.06 GPa, while Young's modulus predicted by the unit cell (used in Section 3.2.1) is 89.35 GPa. Evaluating the difference, this value is lower than 2%.

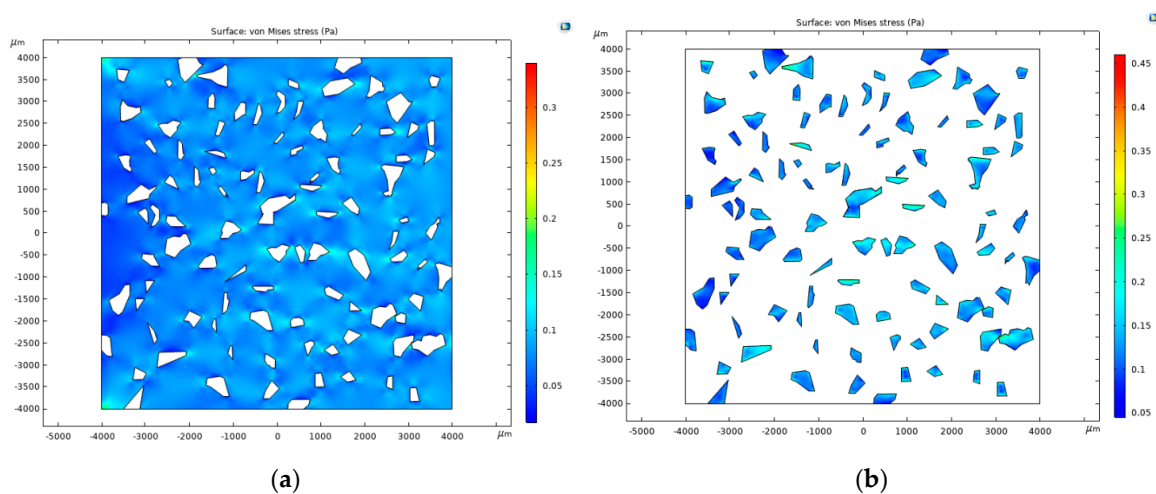


Figure 14. Von Mises stress distribution in (a) matrix and (b) particles. Constituents are fully dense.

Figure 15a,b show the surface plots of von Mises stress in the porous Al-matrix and the SiC particles (some particles are porous), respectively. The presence of the pores within the composite

produces higher stress in the matrix as well as in the particles, but the particles are under higher stress when compared to the fully dense composite, indicating that the particles undergoing increased loads. The stress is concentrated in the poles of the pores, in the sharp angular corners of the particles and at the contact points among the particle, matrix, and pore. The Young's modulus of this porous composite is 86.6 GPa. The pore content of 1.2% (volume fraction), reduced the elastic modulus by about 5% (from 91.06 to 86.6 GPa) despite the load transfer is increased. The mechanical behavior observed within the structure of a real composite material under load, is similar to that observed in the results of Sections 3.2.1–3.2.5. Thus, as the results computed with the UCs models are coincident with experimental data, as well as with the results computed by the REV models, the conclusions drawn by this research are confirmed. Therefore, the presence of the pores leads to a relaxation of the composite and reduces its stress gathering capability.

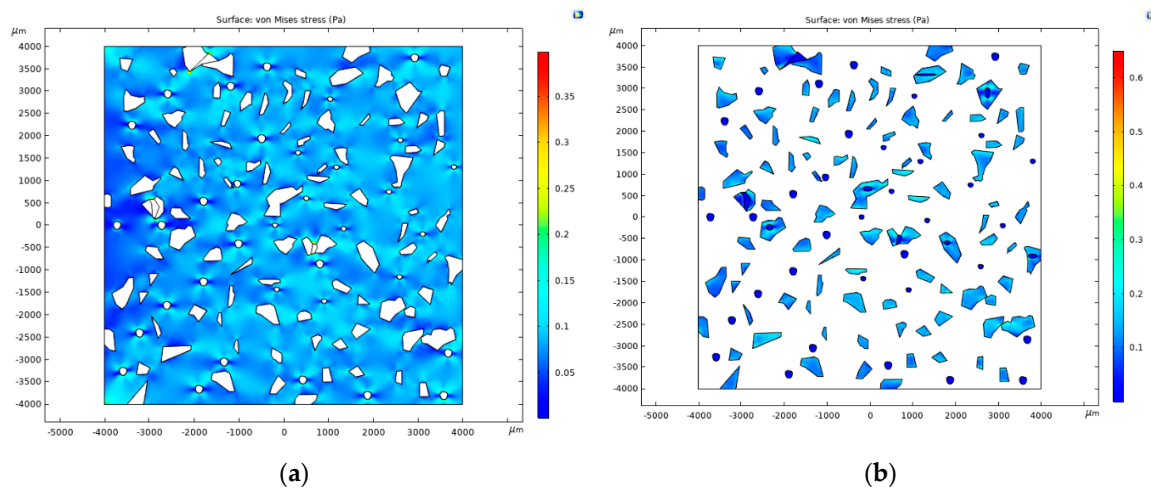


Figure 15. Von Mises stress distribution in (a) matrix and (b) particles. Matrix is porous while particles are both porous and pore free.

4. Conclusions

In the present work, 2D models (UC and REV approaches) and finite element analysis are used to investigate the porosity effect on the SiC particle reinforced Al matrix composites. The reliability of the numerical methodology was validated by comparing the numerical results against several experimental data, micromechanical constitutive models, and structures that represent real composite materials. The main results to be highlighted are as follows:

- (1) In the case of fully dense SiC particles and fully dense Al-matrix, the square and circular particles endure the same load to the volume fraction up to 11%. However, above this reinforcement content, the angular particle endures more load. Therefore, the effective elastic modulus of the MMC is independent of the morphology when the reinforcement content is lower to 11%.
- (2) Despite the presence of pore in the composite, stress transfer from the soft matrix to the hard particle is effective in all cases, except in the case of fully dense circular particle and porous matrix.
- (3) For pores within the particles, the stress concentration around the pore is higher for the circular particles than the square ones.
- (4) The elastic modulus is more sensitive to porosity in the matrix, which is a common defect in MMC.
- (5) For the square or angular particles, the pore within the particle affects the load transfer mechanism in the same way to the pore located at the particle matrix interface.
- (6) For the porosity at the particle–matrix interface, the contact points among the particle, matrix, and the pore acts as a stress concentrator.

- (7) The porosity plays a significant role in the strength of the composites, and for a given porosity in the matrix, it impairs the Young's modulus in the same way independently of the shape of the SiC-reinforcement.

Author Contributions: Conceptualization, J.E.R.-S. and K.M.G.-J.; methodology, J.E.R.-S. and K.M.G.-J.; software, J.E.R.-S.; validation, J.E.R.-S. and K.M.G.-J.; formal analysis, J.E.R.-S.; investigation, J.E.R.-S.; resources, A.C.-R., J.A.R.-S., V.H.G.-P., A.M.-P., and E.H.-H.; data curation, J.E.R.-S.; writing—original draft preparation, J.E.R.-S. and K.M.G.-J.; writing—review and editing, J.E.R.-S., K.M.G.-J., A.C.-R. and A.M.-P.; visualization, J.E.R.-S., K.M.G.-J., A.C.-R., J.A.R.-S., A.M.-P., E.H.-H., and V.H.G.-P.; supervision, J.E.R.-S., A.C.-R., and J.A.R.-S.; project administration, J.E.R.-S.; funding acquisition, J.E.R.-S., K.M.G.-J., A.C.-R., J.A.R.-S., E.H.-H., A.M.-P. and V.H.G.-P. All authors have read and agreed to the published version of the manuscript.

Funding: This research was funded by CONACYT, grant number “A1-S-9692” and “The APC was funded by CONACYT A1-S-9692”.

Acknowledgments: The authors wish to thank the Institutions CONACYT, SNI, Centro de Investigación en Química Aplicada, and Instituto Politécnico Nacional, for their permanent support. J.E. Rivera gratefully acknowledges the financial support received from Cátedras CONACYT project 809.

Conflicts of Interest: The authors declare no conflict of interest.

References

- Arreola-Herrera, R.; Cruz-Ramírez, A.; Rivera-Salinas, J.E.; Romero-Serrano, J.A.; Sánchez-Alvarado, R.G. The effect of non-metallic inclusions on the mechanical properties of 32 CDV 13 steel and their mechanical stress analysis by numerical simulation. *Theor. Appl. Fract. Mech.* **2018**, *94*, 134–146. [[CrossRef](#)]
- Kulkarni, S.G.; Achchhe, L.; Menghani, J.V. Effect of reinforcement type and porosity on strength of metal matrix composite. *Int. J. Comput. Mater. Sci. Eng.* **2016**, *5*, 1650006. [[CrossRef](#)]
- Shen, L.; Finot, M.; Needleman, A.; Suresh, S. Effective plastic response of two-phase composites. *Acta Metall. Mater.* **1995**, *43*, 1701–1722. [[CrossRef](#)]
- Chawla, N.; Chawla, K.K. Microstructure-based modeling of the deformation behavior of particle reinforced metal matrix composites. *J. Mater. Sci.* **2006**, *41*, 913–925. [[CrossRef](#)]
- Nasher, N.; Hori, M. *Micromechanics: Overall Properties of Heterogeneous Materials*, 2nd ed.; Elsevier: North-Holland, The Netherlands, 1999.
- Gentieu, T.; Catapano, A.; Jume, J.; Broughton, J. Computational modeling of particulate-reinforced materials up to high volume fractions: Linear elastic homogenization. *J. Mater. Des. Appl.* **2019**, *233*, 1101–1116.
- Hassani, A.; Bagherpour, E.; Qods, F. Influence of pores on workability of porous Al/SiC composites fabricated through powder metallurgy + mechanical alloying. *J. Alloys Compd.* **2014**, *591*, 132–142. [[CrossRef](#)]
- Schöbel, M.; Requena, G.; Fiedler, G.; Tolnai, D.; Vaucher, S.; Degischer, H.P. Void formation in metal matrix composites by solidification and shrinkage of an AlSi7 matrix between densely packed particles. *Compos. Part A Appl. Sci. Manuf.* **2014**, *66*, 103–108. [[CrossRef](#)]
- Arif, M.N.; Bukhari, M.Z.; Brabazon, D.; Hashmi, M.S.J. Coefficient of thermal expansion (CTE) study in metal matrix composite of CuSiC vs. AlSiC. *IOP Conf. Ser. Mater. Sci. Eng.* **2019**, *701*, 012057. [[CrossRef](#)]
- Podymova, N.B.; Kalashnikov, I.E.; Bolotova, L.K.; Kobeleva, L.I. Laser-ultrasonic nondestructive evaluation of porosity in particulate reinforced metal-matrix composites. *Ultrasonics* **2019**, *99*, 105959. [[CrossRef](#)]
- Schöbel, M.; Altendorfer, W.; Degischer, H.P.; Vaucher, S.; Buslaps, T.; Di Michiel, M.; Hofmann, M. Internal stresses and voids in SiC particle reinforced aluminum composites for heat sink applications. *Compos. Sci. Technol.* **2011**, *71*, 724–733. [[CrossRef](#)]
- Voigt, W. Über die Beziehung zwischen den beiden Elastizitätskonstanten Isotroper Körper. *Wied. Ann. Phys.* **1889**, *38*, 573–587. [[CrossRef](#)]
- Reuss, A. Berechnung der Fließgrenze von Mischkristallen auf Grund der Plastizitätsbedingung für Einkristalle. *J. Appl. Math. Mech.* **1929**, *9*, 49–58.
- Hashin, Z.; Shtrikman, S. A variational approach to the theory of the elastic behavior of multiphase materials. *J. Mech. Phys. Solids* **1963**, *11*, 127–140. [[CrossRef](#)]
- Ramakrishnan, N.; Arunachalam, V. Effective elastic moduli of porous solids. *J. Mater. Sci.* **1990**, *25*, 3930–3937. [[CrossRef](#)]
- Ramakrishnan, N.; Arunachalam, V. Effective elastic moduli of porous ceramic materials. *J. Am. Ceram. Soc.* **1993**, *76*, 2745–2752. [[CrossRef](#)]

17. Chawla, N.; Shen, Y. Mechanical behavior of particle reinforced metal matrix composites. *Adv. Eng. Mater.* **2001**, *6*, 357–370. [[CrossRef](#)]
18. Chawla, N.; Ganesh, V.; Wunsch, B. Three-dimensional (3D) microstructure visualization and finite element modeling of the mechanical behavior of SiC particle reinforced aluminum composites. *Scr. Mater.* **2004**, *51*, 161–165. [[CrossRef](#)]
19. Dong, C. Effects of process-induced voids on the properties of fibre reinforced composites. *J. Mater. Sci. Technol.* **2016**, *32*, 597–604. [[CrossRef](#)]
20. Deng, X.; Koopman, M.; Chawla, K.K.; Scarritt, S. Measurement and prediction of Young's modulus of a Pb-free solder. *J. Mater. Sci. Mater. Electron.* **2004**, *15*, 385–388.
21. Kukshal, V.; Gangwar, S.; Patnaik, A. Experimental and finite element analysis of mechanical and fracture behavior of SiC particulate filled A356 alloy composites: Part I. *J. Mater. Des. Appl.* **2015**, *229*, 91–105. [[CrossRef](#)]
22. Hashim, J.; Looney, M.; Hashmi, M.S.J. The enhancement of wettability of SiC particles in cast aluminum matrix composites. *J. Mater. Process. Technol.* **1999**, *1*, 329–335.
23. Ray, S. Review Synthesis of cast metal matrix particulate composite. *J. Mater. Sci.* **1993**, *28*, 539–5413. [[CrossRef](#)]
24. Sun, C.; Song, M.; Wang, Z.; He, Y. Effect of particle size on the microstructures and mechanical properties of SiC-reinforced pure aluminum composites. *J. Mater. Eng. Perform.* **2011**, *20*, 1606–1612. [[CrossRef](#)]
25. Koopman, M.; Chawla, K.K.; Coffin, C.; Patterson, B.R.; Deng, X.; Patel, B.V.; Fang, Z.; Lockwood, G. Determination of elastic constants in WC/Co metal matrix composites by resonant ultrasound spectroscopy and impulse excitation. *Adv. Eng. Mater.* **2002**, *4*, 37–42. [[CrossRef](#)]
26. Eroshkin, O.; Tsukrov, I. On micromechanical modeling of particulate composites with inclusions of various shapes. *Int. J. Solids Struct.* **2005**, *42*, 409–427. [[CrossRef](#)]
27. Fish, J.; Belytschko, T. *A Fist Course in Finite Elements*; John Wiley and Sons, Ltd.: Hoboken, NJ, USA, 2007.
28. Sun, C.T.; Vaidya, R.S. Prediction of composite properties from a representative volume element. *Compos. Sci. Technol.* **1996**, *56*, 171–179. [[CrossRef](#)]
29. Tillmann, W.; Klusemann, B.; Nebel, J.; Svendsen, B. Analysis of the mechanical properties of an Arc-sprayed WC-FeCSiMn coating: Nanoindentation and simulation. *J. Therm. Spray Technol.* **2011**, *20*, 328–335. [[CrossRef](#)]
30. Ganesh, V.V.; Chawla, N. Effect of particle orientation anisotropy on the tensile behavior of metal matrix composites: Experiments and microstructure-based simulation. *Mater. Sci. Eng. A* **2005**, *391*, 342–353. [[CrossRef](#)]
31. Clayne, T.W.; Withers, P.J. *An Introduction to Metal Matrix Composites*; Cambridge University Press: Cambridge, UK, 1995.
32. McDaniels, D.L. Analysis of stress-strain, fracture, and ductility behavior of aluminum matrix composites containing discontinuous silicon carbide reinforcement. *Metall. Trans. A* **1985**, *16*, 1105–1115. [[CrossRef](#)]
33. Upadhy, A.; Ramvir, S. Prediction of effective elastic modulus of biphasic composite materials. *Mod. Mech. Eng.* **2012**, *2*, 6–13. [[CrossRef](#)]
34. Qu, S.G.; Lou, H.S.; Li, X.Q. Influence of particle size distribution on properties of SiC particles reinforced aluminum matrix composites with high SiC particle content. *J. Compos. Mater.* **2016**, *50*, 1049–1058. [[CrossRef](#)]
35. Sherif El-Eskandarany, M. Mechanical solid state mixing for synthesizing of SiCp/Al nanocomposites. *J. Alloys Compd.* **1998**, *279*, 263–271. [[CrossRef](#)]
36. Santhosh Kumar, S.; Seshu Bai, V.; Rajkumar, K.V.; Sharma, G.K.; Jayakumar, T.; Rajasekharan, T. Elastic modulus of Al–Si/SiC metal matrix composites as a function of volume fraction. *J. Phys. D Appl. Phys.* **2009**, *42*, 175504. [[CrossRef](#)]
37. Liaw, P.K.; Shannon, R.E.; Clark, W.G.; Harrigan, W.C.; Jeong, H.; Hsu, D.K. Nondestructive characterization of material properties of metal-matrix composites. *Mater. Chem. Phys.* **1995**, *39*, 220–228. [[CrossRef](#)]

